

Porosity effect on unsteady MHD free convection flow of Jeffrey fluid past an oscillating vertical plate with ramped wall temperature

Nor Athirah Mohd Zin^a, Ahmad Qushairi Mohamad^a, Ilyas Khan^b, Sharidan Shafie^{a,*}

^a Department of Mathematical Sciences, Universiti Teknologi Malaysia, Skudai 81310 UTM Johor Bahru, Johor, Malaysia

^b Basic Sciences Department, College of Engineering Majmaah University, P.O. Box 66, Majmaah 11952, Saudi Arabia

* Corresponding author: sharidan@utm.my

Article history

Received 22 January 2017

Accepted 22 Mac 2017

Abstract

The unsteady magnetohydrodynamic (MHD) free convection flow of Jeffrey fluid embedded in porous medium past an oscillating vertical plate generated by thermal radiation with ramped wall temperature is investigated. The incompressible fluid is taken electrically conducting under the action of transverse magnetic field towards the flow. Constitutive relation of Jeffrey fluid is employed to model the governing equations in terms of partial differential equations with some physical conditions. The transformed dimensionless governing equations are solved analytically using Laplace transform technique. The impact of various pertinent parameters namely material parameter of Jeffrey fluid λ_1 , dimensionless parameter of Jeffrey fluid λ , phase angle ωt , Hartmann number

Ha , permeability parameter K , Grashof number Gr , Prandtl number Pr , radiation parameter Rd and dimensionless time t on velocity and temperature distributions are presented graphically and discussed in details. It is observed that, the permeability parameter tend to retard the fluid velocity for ramped wall temperature but enhance the velocity for an isothermal plate. Besides that, this study shows, the amplitude of velocity and temperature fields for ramped wall temperature are always lower than isothermal plate. A comparison with the existing published work is also provided to confirm the validity of the present results and an excellent agreement are identical.

Keywords: Unsteady Jeffrey fluid, MHD, porous medium, oscillating vertical plate, Laplace transform technique

© 2017 Penerbit UTM Press. All rights reserved

INTRODUCTION

During the last decades, considerable amount of efforts have been made in the study of non-Newtonian fluid because of their wide and practical applications in various branches of sciences and engineering, for instance in wire and blade coating, plastics manufacturing, dying of papers and textiles, food processing and movement of biological fluids. However, such flows are not possible to describe by a single constitutive relation between shear stress and rate of strain. Keeping this fact in mind, many models has been introduced in the literature to predict the rheological behavior of non-Newtonian fluids. Amongst them, Jeffrey model is accorded as a relatively simpler linear model which time derivatives are used instead of convected derivatives. The Jeffrey model has received special attentions from the researchers including Khan (2007), Hayat *et al.* (2010), Mekheimer *et al.* (2011), Khan *et al.* (2011), Qayyum *et al.* (2012) and so on.

The influence of heat transfer on mixed convection of MHD oscillatory flow of Jeffrey fluid in a channel has been explored by Kavita *et al.* (2012). In a subsequent year, Idowu *et al.* (2013) expended the previous idea of Kavita *et al.* (2012) by considered the mass transfer and chemical reaction into the unsteady mixed convection of MHD oscillatory flow of Jeffrey fluid in a horizontal channel and performed an exact solutions for velocity, temperature and concentration using

perturbation technique. Ali and Asghar (2014) analytically examined the two-dimensional oscillatory flow inside a rectangular channel for Jeffrey fluid with small suction using several methodologies namely perturbation technique, Wentzel-Kramers-Brillouin and variation of parameter. Nadeem *et al.* (2014) further studied the unsteady oscillatory stagnation point flow of a Jeffrey fluid using Homotopy Analysis Method (HAM).

In another paper, Idowu *et al.* (2015a) worked on the effect of heat and mass transfer on MHD oscillatory flow of Jeffrey fluid through a porous medium in a channel in the presence of thermal conductivity, thermal radiation and so on. The partial differential equations are reduced to nonlinear ordinary differential equation by perturbation technique and hence solved numerically by using shooting technique with fourth order Runge-Kutta method. In the same year, Idowu *et al.* (2015b) continued their previous work with heat absorption and dufour effect and solved numerically by semi implicit finite difference scheme. Recently, Al-Khafajy (2016) studied analytically the influence of heat transfer on MHD oscillatory flow of Jeffrey fluid with variable viscosity model through porous medium by using perturbation technique. Joseph *et al.* (2016) applied the perturbation technique and analyzed the effect of variable suction on unsteady MHD oscillatory flow of Jeffrey fluid in a horizontal channel with heat and mass transfer. Other than that, a closed form solution for the effect of heat transfer on

unsteady MHD and radiative oscillatory flow of Jeffrey fluid in an inclined channel filled with porous medium and non-uniform walls are carried out by Sree et al. (2016).

On the other hand, some relevant research studies on unsteady Jeffrey fluid past a vertical stretching/shrinking surface by considering different aspects of the problem can be found in Hayat and Mustafa, (2010), Hayat et al. (2014), Mabood et al. (2016) and Sukumar et al. (2016). Nevertheless, Bhaskar Reddy et al. (2015) made an attempt to study the flow of Jeffrey fluid between two torsionally oscillating disks and found that the radial axial flow has a mean steady component and a fluctuating component of frequency twice that of the oscillating disk. Meanwhile, Gao and Jian (2015) proposed the analytic solutions for MHD flow of Jeffrey fluid in a circular microchannel with the aid of separation of variable method, whereas Khan (2015) used the Laplace transformation technique to investigate the unsteady natural convection flow of Jeffrey fluid past an infinite isothermal vertical plate.

Motivated by the above mentioned works and up to the best of author's knowledge no study has been reported concerning the unsteady MHD free convection flow of Jeffrey fluid past an oscillating vertical plate immersed in a porous medium with ramped wall temperature in the presence of magnetic field and thermal radiation effects. Hence, the main purpose of the current study is to provide an exact solution for the simultaneous effects of porosity and magnetic field on unsteady MHD free convection flow of incompressible Jeffrey fluid over an oscillating vertical plate with ramped wall temperature under influence of thermal radiation by Laplace transform technique. Results of involved parameters for velocity and temperature profiles are plotted with the aid of Mathcad software and discussed in details. A comparative study with the existing published work is also provided where an excellent agreement is noticed.

MATHEMATICAL FORMULATION

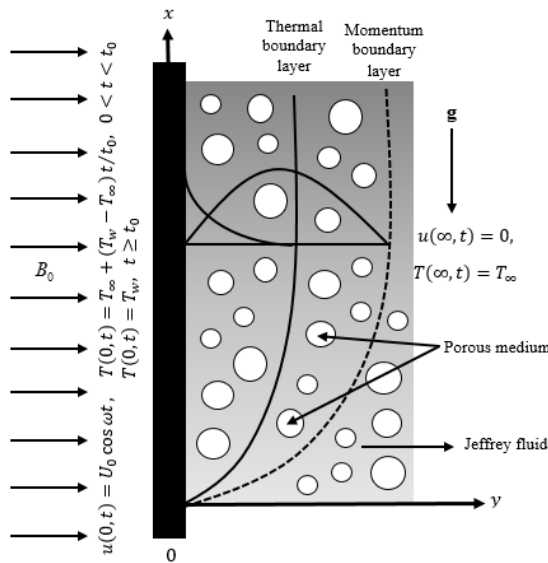


Fig. 1 Schematic diagram of Jeffrey fluid past over an oscillating vertical plate embedded in porous medium.

Consider the unsteady MHD free convection flow of incompressible Jeffrey fluid past an oscillating vertical plate saturated in porous medium under influence of thermal radiation. The *x*-axis is taken along the vertical plate in upward direction, while the *y*-axis is normal to it. The fluid is electrically conducting in the presence of uniform transverse applied magnetic field, *B*₀ parallel to the *y*-axis. The geometrical configuration of the present problem as illustrated in Fig. 1.

The magnetic Reynold number is chosen to be small, so that the induced magnetic field are negligible compared with the applied magnetic field (Aaiza et al., 2015; Khan, 2007). Further, it is also assumed that no polarization and applied voltage exist which means no external electric field and electric field present (Hayat et al., 2010; Gul

et al., 2015). Initially, for time *t* ≤ 0 both the plate and fluid are at rest at constant temperature, *T*_∞ in a stationary condition. After *t* > 0, the plate starts an oscillatory motion in its plane with velocity,

$$u = U_0 H(t) \cos \omega t, \tag{1}$$

against the gravitational field, where *U*₀ is the amplitude of the plate oscillation, *H*(*t*) is the Heaviside step function and *ω* is the frequency of the plate oscillations. At the same time, the temperature of the plate is raised or lowered to *T*_∞ + (*T*_w - *T*_∞) *t*/*t*₀ when *t* ≤ *t*₀. Thereafter, at *t* > *t*₀ is maintained at uniform temperature, *T*_w.

Under the above mentioned assumptions and applying the usual Boussinesq approximation (Ghara et al., 2012), the problem is governed by the set of partial differential equations

$$\begin{aligned} \rho \frac{\partial u}{\partial t} &= \frac{\mu}{1 + \lambda_1} \left(1 + \lambda_2 \frac{\partial}{\partial t} \right) \frac{\partial^2 u}{\partial y^2} - \sigma B_0^2 u - \frac{\mu \phi_1}{\kappa (1 + \lambda_1)} \left(1 + \lambda_2 \frac{\partial}{\partial t} \right) u \\ &+ \rho g \beta_r (T - T_\infty), \\ \rho c_p \frac{\partial T}{\partial t} &= k \frac{\partial^2 T}{\partial y^2} - \frac{\partial q_r}{\partial y}, \end{aligned} \tag{2}$$

with the relevant initial and boundary conditions

$$\begin{aligned} u(y, 0) &= 0, \quad T(y, 0) = T_\infty; \quad y \geq 0, \\ u(0, t) &= U_0 H(t) \cos \omega t; \quad t > 0, \\ T(0, t) &= T_\infty + (T_w - T_\infty) \frac{t}{t_0}; \quad 0 < t < t_0, \quad T(0, t) = T_w; \quad t \geq t_0, \\ u(\infty, t) &= 0, \quad T(\infty, 0) = T_\infty; \quad t > 0. \end{aligned} \tag{4}$$

Here, *u* denotes the fluid velocity in *x* - direction, *T* is the fluid temperature, *ρ* is the constant density of the fluid, *μ* is the dynamic viscosity, *λ*_{1,2} are the material parameters of the Jeffrey fluid, where *λ*₁ is the ratio of relaxation to retardation times and *λ*₂ is the retardation time, *σ* is the electric conductivity of the fluid, *φ*₁ is the porosity, *κ* is the permeability of the porous medium, *g* is the acceleration due to gravity, *β*_r is the volumetric coefficient of heat transfer, *c*_p is the specific heat capacity, *k* is the thermal conductivity and *q*_r is the radiation heat flux, respectively.

Following Narahari and Ishak (2011), the radiation heat flux under Rosseland approximation is as follows

$$q_r = - \frac{4\sigma^*}{3k_1} \frac{\partial T^4}{\partial y}, \tag{5}$$

where *σ*^{*} denotes the Stefan-Boltzmann and *k*₁ is the absorption coefficient. Assuming the temperature differences within the flow are sufficiently small, such that *T*⁴ is a linear temperature function which can be expanded by Taylor series expansion about *T*_∞. Hence, neglecting higher order terms takes the form

$$T^4 \approx 4T_\infty^3 T - 3T_\infty^4, \tag{6}$$

In view of equations (5) and (6), therefore equation (3) is simplified to

$$\rho c_p \frac{\partial T}{\partial t} = k \left(1 + \frac{16\sigma^* T_\infty^3}{3k_1} \right) \frac{\partial^2 T}{\partial y^2}. \tag{7}$$

Introducing the following dimensionless variables (Ali et al., 2014; Das and Neog, 2015; Khalid et al. 2015)

$$u^* = \frac{u}{U_0}, \quad y^* = \frac{yU_0}{\nu}, \quad t^* = \frac{tU_0^2}{\nu}, \quad \omega^* = \frac{\omega\nu}{U_0^2}, \quad \theta = \frac{T - T_\infty}{T_w - T_\infty}, \quad (8)$$

into equations (2), (7) and (4) yields the following dimensionless expressions (* notations are dropped for simplicity)

$$\frac{\partial u}{\partial t} = \frac{1}{1 + \lambda_1} \left(1 + \lambda \frac{\partial}{\partial t} \right) \frac{\partial^2 u}{\partial y^2} - Hau - \frac{1}{K(1 + \lambda_1)} \left(1 + \lambda \frac{\partial}{\partial t} \right) u + Gr\theta, \quad (9)$$

$$Pr \frac{\partial \theta}{\partial t} = (1 + Rd) \frac{\partial^2 \theta}{\partial y^2}. \quad (10)$$

The adequate initial and boundary conditions in non-dimensional form are

$$\begin{aligned} u(y, 0) &= 0, & \theta(y, 0) &= 0; & y &\geq 0, \\ u(0, t) &= H(t) \cos \omega t, & \theta(0, t) &= t; & 0 < t \leq 1, & \theta(0, t) = 1; & t > 1, \\ u(\infty, 0) &= 0, & \theta(\infty, t) &= 0; & t > 0. \end{aligned} \quad (11)$$

Here,

$$\begin{aligned} \lambda &= \frac{\lambda_2 U_0^2}{\nu}, & \frac{1}{K} &= \frac{\phi \nu^2}{\kappa U_0^2}, & Ha &= \frac{\sigma B_0^2 \nu}{\rho U_0^2}, \\ Gr &= \frac{g \beta_T \nu (T_w - T_\infty)}{U_0^3}, & Pr &= \frac{\mu c_p}{k}, & Rd &= \frac{16 \sigma^* T_\infty^3}{3kk_1}. \end{aligned} \quad (12)$$

In which λ is refer to dimensionless Jeffrey fluid parameter, K is the permeability parameter, Ha is the Hartmann number, Gr is Grashof number, Pr is the Prandtl number and Rd is the radiation parameter, respectively.

SOLUTION OF THE PROBLEM

In order to obtain the analytical solutions for the coupled partial differential equations (9) and (10) under conditions (11), the Laplace transform technique is used. Thus, applying the Laplace transform to equations (9)-(10) and using initial conditions, the following equations in (y, q) are:

$$\frac{d^2 \bar{u}(y, q)}{dy^2} - \left(\frac{\alpha_4 + \alpha_1 q}{\alpha_2 + \alpha_3 q} \right) \bar{u}(y, q) = -\frac{Gr}{\alpha_2 + \alpha_3 q} \bar{\theta}(y, q), \quad (13)$$

$$\frac{d^2 \bar{\theta}(y, q)}{dy^2} - \left(\frac{Pr}{1 + Rd} \right) q \bar{\theta}(y, q) = 0, \quad (14)$$

with transformed boundary conditions

$$\bar{u}(0, q) = \frac{q}{q^2 + \omega^2}, \quad \bar{u}(\infty, q) = 0, \quad (15)$$

$$\bar{\theta}(0, q) = \frac{1 - e^{-q}}{q^2}, \quad \bar{\theta}(\infty, q) = 0, \quad (16)$$

where $\bar{u}(y, q)$ and $\bar{\theta}(y, q)$ indicate the Laplace transform of $u(y, t)$ and $\theta(y, t)$, respectively. The arbitrary constants $\alpha_1, \alpha_2, \alpha_3$ and α_4 are given by

$$\begin{aligned} \alpha_1 &= 1 + \frac{\lambda}{K(1 + \lambda_1)}, & \alpha_2 &= \frac{1}{1 + \lambda_1}, \\ \alpha_3 &= \frac{\lambda}{1 + \lambda_1}, & \alpha_4 &= Ha + \frac{1}{K(1 + \lambda_1)}. \end{aligned} \quad (17)$$

By taking equation (16) into equation (14), yield the following expression

$$\bar{\theta}(y, q) = (1 - e^{-q}) \frac{1}{q^2} e^{-y\sqrt{q_1}}, \quad (18)$$

where

$$q_1 = \frac{Pr}{1 + Rd}. \quad (19)$$

Using the second shift property (Samiulhhaq et al., 2014a)

$$L^{-1} \{ e^{-aq} F(q) \} = f(t - a) H(t - a) \quad \text{if } f(t) = L^{-1} \{ F(q) \}, \quad (20)$$

and expressing

$$\begin{aligned} \theta_R(y, t) &= L^{-1} \left\{ \frac{1}{q^2} e^{-y\sqrt{q_1}} \right\} \\ &= \left(\frac{a_1 y^2}{2} + t \right) \operatorname{erfc} \left(\frac{y}{2} \sqrt{\frac{a_1}{t}} \right) - y \sqrt{\frac{a_1 t}{\pi}} e^{-\frac{a_1 y^2}{4t}}. \end{aligned} \quad (21)$$

Thus, the result for temperature profile can be written as

$$\theta(y, t) = \theta_R(y, t) - \theta_R(y, t - 1) H(t - 1), \quad (22)$$

where L^{-1} denoting the inverse Laplace transform, $H(t - 1)$ is the Heaviside unit step function and $\operatorname{erfc}(\cdot)$ is the complimentary error function.

Then, inserting equation (18) into equation (13) subject to boundary conditions (15), result in

$$\bar{u}(y, q) = \bar{u}_1(y, q) + \bar{u}_2(y, q), \quad (23)$$

where

$$\bar{u}_1(y, q) = \frac{q}{q^2 + \omega^2} e^{-y\sqrt{\frac{\alpha_4 + \alpha_1 q}{\alpha_2 + \alpha_3 q}}}, \quad (24)$$

$$\bar{u}_2(y, q) = \frac{b_4}{(q + b_5)^2 - b_6^2} \frac{(1 - e^{-q})}{q^2} \left[e^{-y\sqrt{\frac{\alpha_4 + \alpha_1 q}{\alpha_2 + \alpha_3 q}}} - e^{-y\sqrt{q_1}} \right], \quad (25)$$

in which

$$b_4 = \frac{Gr}{a_1 \alpha_3}, \quad b_5 = \frac{a_1 \alpha_2 - \alpha_1}{2a_1 \alpha_3}, \quad b_6 = \frac{\sqrt{(a_1 \alpha_2 - \alpha_1)^2 + 4a_1 \alpha_3 \alpha_4}}{2a_1 \alpha_3}. \quad (26)$$

Now to determine the inverse Laplace of equation (24), we split equation (24) in the following form

$$\bar{u}_1(y, q) = \bar{G}_{11}(q) \cdot \bar{G}_{12}(y, q), \quad (27)$$

where

$$\bar{G}_{11}(q) = \frac{q}{q^2 + \omega^2}, \quad (28)$$

$$\bar{G}_{12}(y, q) = e^{-y\sqrt{\frac{\alpha_4 + \alpha_1 q}{\alpha_2 + \alpha_3 q}}}. \quad (29)$$

Inverting equation (28) gives

$$G_{11}(t = H t) \cos \omega t, \tag{30}$$

and applying the inversion formula of compound function (Khan et al., 2010) to equation (29), leads to the following expression

$$G_{12}(y, t = \delta(t) e^{-y\sqrt{L_5}}) + \int_0^t \frac{y}{2u\sqrt{\pi u}} \sqrt{\frac{L_6}{t}} e^{-\frac{y^2}{4u} - L_4 t - uL_5} I_1(2\sqrt{L_6 u t}) du, \tag{31}$$

with

$$L_4 = \frac{\alpha_2}{\alpha_3}, \quad L_5 = \frac{\alpha_1}{\alpha_3}, \quad L_6 = \frac{\alpha_1 L}{\alpha_3}. \tag{32}$$

Here $\delta(t)$ is a delta function and $I_1(\cdot)$ is the modified Bessel function of the first kind of order one. Since $\bar{u}_1(\cdot)$ involved of multiplication of two functions, then the convolution theorem is used

$$u_1(\cdot, \cdot) = \int_0^t f(t-\tau) g(\tau) d\tau \tag{33}$$

thus,

$$u_1(y, t = H t) e^{-y\sqrt{L_5}} \cos \omega t + \frac{H(t)}{2} \sqrt{\frac{L_6}{\pi}} \int_0^t \frac{y \cos \omega(t-s)}{u\sqrt{s}} e^{-\frac{y^2}{4u} - L_4 s - L_5} I_1(2\sqrt{L_6 u s}) duds. \tag{34}$$

In order to find the solution for $\bar{u}_2(\cdot, \cdot)$, we write equation (25) as follow

$$\bar{u}_2(\cdot, \cdot) = (-y)^{-2} (1)^{-1} (q) \tag{35}$$

where

$$\bar{u}_{21}(q) = \frac{b_4}{(q + b_5)^2 - b_6^2}, \tag{36}$$

$$\bar{u}_{22}(y, q) = \frac{1}{q^2} \left[e^{-y\sqrt{\frac{\alpha_4 + \alpha_1 q}{\alpha_2 + \alpha_3 q}}} - e^{-y\sqrt{\alpha_1 q}} \right]. \tag{37}$$

The inverse Laplace of equation (36) is

$$u_2(t = \frac{b_4}{b_6} e^{-b_5 t}) s^{-2} (b_6 t) \tag{38}$$

Rewrite equation (37) into two set of functions, and let

$$\bar{A}_1(y, q) = \frac{1}{q^2} e^{-y\sqrt{\frac{\alpha_4 + \alpha_1 q}{\alpha_2 + \alpha_3 q}}}, \tag{39}$$

$$\bar{A}_2(y, q) = \frac{1}{q^2} e^{-y\sqrt{\alpha_1 q}}. \tag{40}$$

Here, $A_1(\cdot, \cdot)$ can be presented as a convolution product

$$A_1(\cdot, \cdot) = \int_0^t f(t-\tau) g(\tau) d\tau \tag{41}$$

where

$$G_{13}(t = L^{-1} \left\{ \frac{1}{q^2} \right\}) = t, \tag{42}$$

and the function of $G_{12}(y, t)$ is already calculated in equation (31), whereas the inverse Laplace transform of $\bar{A}_2(\cdot, \cdot)$ is same as in equation (21). Hence, using equations (31) and (42), the solution of equation (39) results

$$A_1(y, t = t e^{-y\sqrt{L_5}}) + \frac{1}{2} \sqrt{\frac{L_6}{\pi}} \int_0^t \int_0^{\infty} \frac{y(t-s)}{u\sqrt{s}} e^{-\frac{y^2}{4u} - L_4 s - L_5} I_1(2\sqrt{L_6 u s}) duds. \tag{43}$$

Thus, $u_{22}(y, t)$ implies

$$u_{22}(y, t = t e^{-y\sqrt{L_5}}) + \frac{1}{2} \sqrt{\frac{L_6}{\pi}} \int_0^t \int_0^{\infty} \frac{y(t-s)}{u\sqrt{s}} e^{-\frac{y^2}{4u} - L_4 s - L_5} I_1(2\sqrt{L_6 u s}) duds - \left(\frac{a_1 y^2}{2} + t \right) \operatorname{erfc} \left(\frac{y}{2} \sqrt{\frac{a_1}{t}} \right) + y \sqrt{\frac{a_1 t}{\pi}} e^{-\frac{a_1 y^2}{4t}}. \tag{44}$$

Again, using the second shift property, the solution of equation (25) can be obtained as

$$u_2(y, t = u_R y) - u_R y t - (H t) \tag{45}$$

where $u_R(\cdot, \cdot)$ can be determined by the convolution theorem, hence

$$u_R(y, t = u_{21} \otimes u_{22}) = \int_0^t u_{21}(t-\ell) u_{22}(y, \ell) d\ell = \frac{b_4}{b_6} \int_0^t \ell e^{b_5(\ell-t) - y\sqrt{L_5}} \sinh[b_6(t-\ell)] d\ell + \frac{b_4}{2b_6} \sqrt{\frac{L_6}{\pi}} \int_0^t \int_0^{\infty} \int_0^{\infty} \frac{y(\ell-s)}{u\sqrt{s}} e^{b_5(\ell-t) - \frac{y^2}{4u} - L_4 s - uL_5} \times \sinh[b_6(t-\ell)] I_1(2\sqrt{L_6 u s}) duds d\ell - \frac{b_4}{b_6} \int_0^t e^{b_5(\ell-t)} \sinh[b_6(t-\ell)] \times \left(\frac{a_1 y^2}{2} + \ell \right) \operatorname{erfc} \left(\frac{y}{2} \sqrt{\frac{a_1}{\ell}} \right) d\ell + \frac{b_4}{b_6} \sqrt{\frac{a_1}{\pi}} \int_0^t y \sqrt{\ell} e^{b_5(\ell-t) - \frac{a_1 y^2}{4\ell}} \sinh[b_6(t-\ell)] d\ell. \tag{46}$$

Consequently, the complete solution for velocity distribution is given by

$$u(y, t = u_1(y, t) + u_R(y, t) - u_R(y, t) - (H t)) \tag{47}$$

Solution for an isothermal plate

In order to highlight the effect of ramped temperature distribution of the plate on the fluid flow, the same problem subjected to the constant wall temperature are solved, and both solutions are compared. The solutions for temperature and velocity profiles for the case of an isothermal plate can be expressed as

$$\theta(y, t = \operatorname{erfc} \left(\frac{y}{2} \sqrt{\frac{a_1}{t}} \right), \tag{48}$$

$$\begin{aligned}
 u(y,t) = & H(t) \cos \omega t \left(\right) \\
 & + \frac{H(t)}{2} \sqrt{\frac{L_6}{\pi}} \int_0^t \int_0^\infty \frac{y \cos \omega(t-s)}{u \sqrt{s}} e^{-\frac{y^2-L_4 s}{4u}} I_1(2\sqrt{L_6 u s}) \, duds \\
 & + \frac{b_4}{b_6} \int_0^t e^{b_5(t-y)\sqrt{L_6}} \sinh[b_6(t-\ell)] \, d\ell \\
 & + \frac{b_4}{2b_6} \sqrt{\frac{L_6}{\pi}} \int_0^t \int_0^\infty \frac{y}{u \sqrt{s}} e^{-\frac{b_5(\ell-t)-L_4 s-uL}{4u}} \\
 & \quad \times I_1(2\sqrt{L_6 u s}) \sinh[b_6(t-\ell)] \, duds \, d\ell \\
 & - \frac{b_4}{b_6} \int_0^t e^{b_5(\ell-t)} \sinh[b_6(t-\ell)] \operatorname{erfc}\left(\frac{y}{2\sqrt{\frac{a_1}{\ell}}}\right) \, d\ell,
 \end{aligned} \tag{49}$$

respectively.

Nusselt number and skin friction

In this section, the expression of Nusselt number, Nu and skin friction τ for both cases, ramped wall temperature and an isothermal plate are discussed. The dimensionless Nusselt number and skin friction are defined as

$$Nu = -\left. \frac{\partial \theta}{\partial y} \right|_{y=0}, \tag{50}$$

$$\tau = \frac{1}{1+\lambda_1} \left(1 + \lambda \frac{\partial}{\partial t} \right) \left. \frac{\partial u}{\partial y} \right|_{y=0}. \tag{51}$$

Substituting equations (22) and (48) into (50), thus the Nusselt number for ramped wall temperature and isothermal are given by

$$\begin{aligned}
 N_{r} &= 2\sqrt{\frac{a_1}{\pi}} \left[\sqrt{t} - \sqrt{-1} \right] \dots \tag{52} \\
 Nu_{iso} &= \sqrt{\frac{a_1}{\pi t}}. \tag{53}
 \end{aligned}$$

While, introducing equations (47) and (49) into (51), the skin friction for both ramped wall temperature and constant wall temperature can be written as

$$\tau_r = \dots \tag{54}$$

and

$$\tau_{iso} = \tau_1(t + \tau_3 t), \tag{55}$$

where $\tau_i (i=1, \dots)$ are given by

$$\begin{aligned}
 \tau_1 = & H(t) \sqrt{L_5} (-\alpha_2) \cos \omega t + \alpha_3 \omega \sin \omega t \\
 & + \frac{H(t)}{2} \sqrt{\frac{L_6}{\pi}} \int_0^t \int_0^\infty \frac{y \cos \omega(t-s)}{u \sqrt{s}} e^{-\frac{y^2-L_4 s-uL}{4u}} \\
 & \times [\alpha_2 \cos \omega(t-s) - \alpha_3 \omega \sin \omega(t-s)] I_1(2\sqrt{L_6 u s}) \, duds,
 \end{aligned} \tag{56}$$

$$\begin{aligned}
 \tau_R = & -\alpha_2 \sqrt{L_5} \int_0^t \ell e^{b_5(\ell-t)} \left\{ \frac{b_4}{b_6} (\lambda b_5 - 1) \sinh[b_6(\ell-t)] \right. \\
 & \left. + \lambda b_4 \cosh[b_6(\ell-t)] \right\} \, d\ell \\
 & + \frac{\alpha_2}{2} \sqrt{\frac{L_6}{\pi}} \int_0^t \int_0^\infty \frac{(\ell-s)}{u \sqrt{s}} e^{b_5(\ell-t)-L_4 s-uL} I_1(2\sqrt{L_6 u s}) \times \\
 & \left\{ \frac{b_4}{b_6} (\lambda b_5 - 1) \sinh[b_6(\ell-t)] \right. \\
 & \left. + \lambda b_4 \cosh[b_6(\ell-t)] \right\} \, duds \, d\ell \\
 & + 2\alpha_2 \sqrt{\frac{a_1}{\pi}} \int_0^t \sqrt{\ell} e^{b_5(\ell-t)} \left\{ \frac{b_4}{b_6} (\lambda b_5 - 1) \sinh[b_6(\ell-t)] \right. \\
 & \left. + \lambda b_4 \cosh[b_6(\ell-t)] \right\} \, d\ell,
 \end{aligned} \tag{57}$$

$$\begin{aligned}
 \tau_3 = & -\alpha_2 \sqrt{L_5} \int_0^t e^{b_5(\ell-t)} \left\{ \frac{b_4}{b_6} (\lambda b_5 - 1) \sinh[b_6(\ell-t)] \right. \\
 & \left. + \lambda b_4 \cosh[b_6(\ell-t)] \right\} \, d\ell \\
 & + \frac{\alpha_2}{2} \sqrt{\frac{L_6}{\pi}} \int_0^t \int_0^\infty \frac{1}{u \sqrt{s}} e^{b_5(\ell-t)-L_4 s-uL} I_1(2\sqrt{L_6 u s}) \times \\
 & \left\{ \frac{b_4}{b_6} (\lambda b_5 - 1) \sinh[b_6(\ell-t)] \right. \\
 & \left. + \lambda b_4 \cosh[b_6(\ell-t)] \right\} \, duds \, d\ell \\
 & + \alpha_2 \sqrt{\frac{a_1}{\pi}} \int_0^t \frac{1}{\sqrt{\ell}} e^{b_5(\ell-t)} \left\{ \frac{b_4}{b_6} (\lambda b_5 - 1) \sinh[b_6(\ell-t)] \right. \\
 & \left. + \lambda b_4 \cosh[b_6(\ell-t)] \right\} \, d\ell,
 \end{aligned} \tag{58}$$

respectively.

LIMITING CASES

Case 1: Solution in the absence of MHD, porosity and radiation

By considering $Ha = 0$, $Rd = 0$ and $K \rightarrow \infty$, the correspond solution of velocity profile for ramped wall temperature is reduced to

$$\begin{aligned}
 u_{ramp}(y,t) = & H(t) \cos \omega t e^{-\frac{y}{\sqrt{\alpha_3}}} \left(\right) \\
 & + \frac{H(t)}{2} \sqrt{\frac{L_{16}}{\pi}} \int_0^t \int_0^\infty \frac{y \cos \omega(t-s)}{u \sqrt{s}} e^{-\frac{y^2-L_4 s}{4u}} I_1(2\sqrt{L_{16} u s}) \, duds \\
 & + u_{R1}(y,t) - u_{R1}(y) - 1 - H(t-1),
 \end{aligned} \tag{59}$$

where

$$\begin{aligned}
 u_{R1}(y,t) = & \frac{b_{14}}{b_{15}} \int_0^t \ell e^{b_1(\ell-t)-\frac{y}{\sqrt{\alpha_3}}} \sinh[b_{15}(t-\ell)] \, d\ell \\
 & + \frac{b_{14}}{2b_{15}} \sqrt{\frac{L_{16}}{\pi}} \int_0^t \int_0^\infty \frac{y(\ell-s)}{u \sqrt{s}} e^{b_1(\ell-t)-\frac{y^2}{4u}-L_4 s-\frac{y}{\alpha_3}} \\
 & \quad \times \sinh[b_{15}(t-\ell)] I_1(2\sqrt{L_{16} u s}) \, duds \, d\ell \\
 & - \frac{b_{14}}{b_{16}} \int_0^t e^{b_1(\ell-t)} \sinh[b_{15}(t-\ell)] \left(\frac{\operatorname{Pr} y^2}{2} + \ell \right) \operatorname{erfc}\left(\frac{y}{2\sqrt{\operatorname{Pr}}}\right) \, d\ell \\
 & + \frac{b_{14}}{b_{15}} \sqrt{\frac{\operatorname{Pr}}{\pi}} \int_0^t y \sqrt{\ell} e^{b_1(\ell-t)-\frac{\operatorname{Pr} y^2}{4\ell}} \sinh[b_{15}(t-\ell)] \, d\ell,
 \end{aligned} \tag{60}$$

in which

$$b_{14} = \frac{Gr}{\alpha_3 \operatorname{Pr}}, \quad b_{15} = \frac{\alpha_2 \operatorname{Pr} - 1}{2\alpha_3 \operatorname{Pr}}, \quad L_{16} = \frac{L_4}{\alpha_3}. \tag{61}$$

While, the velocity profile for an isothermal plate is

$$\begin{aligned}
 u_{iso}(y,t) &= H(t) \cos \omega t e^{-\frac{y}{\sqrt{\alpha_3}}} \\
 &+ \frac{H(t)}{2} \sqrt{\frac{L_{16}}{\pi}} \int_0^t \int_0^\infty \frac{y \cos[\omega(t-s)]}{u\sqrt{s}} e^{-\frac{y^2}{4u} - L_4 s - \frac{u}{\alpha_3}} I_1(2\sqrt{L_{16}us}) duds \\
 &+ \frac{b_{14}}{b_{15}} \int_0^t e^{b_{15}(t-\tau)} \frac{y}{\sqrt{\alpha_3}} \sinh[b_{15}(t-\ell)] d\ell \\
 &+ \frac{b_{14}}{2b_{15}} \sqrt{\frac{L_{16}}{\pi}} \int_0^t \int_0^\infty \frac{y}{u\sqrt{s}} e^{b_{15}(t-\tau) - \frac{y^2}{4u} - L_4 s - \frac{u}{\alpha_3}} \\
 &\quad \times \sinh[b_{15}(t-\ell)] I_1(2\sqrt{L_{16}us}) duds d\ell \\
 &- \frac{b_{14}}{b_{15}} \int_0^t e^{b_{15}(t-\tau)} \sinh[b_{15}(t-\ell)] \operatorname{erfc}\left(\frac{y}{2} \sqrt{\frac{\operatorname{Pr}}{\ell}}\right) d\ell.
 \end{aligned} \tag{62}$$

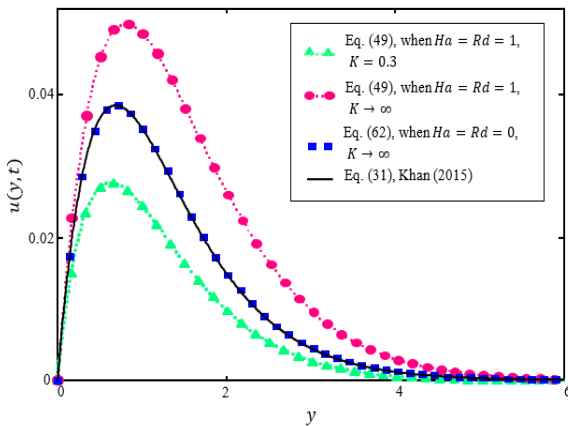


Fig 2. Comparison of velocity profile for an isothermal case in equation (62) with equation (31) obtained by Khan (2015) when $\lambda_1 = \lambda = 1$, $Gr = 0.5$, $Pr = 0.71$ and $t = 0.5$.

Clearly in Fig. 2, the graph of an isothermal plate in equation (62) is matched well with those obtained by Khan (2015). Hence, we can say our present results found are in an excellent agreement.

Case 2: Solution in the absence of λ_1

By taking $\lambda_1 = 0$, the solution of equations (47) and (49) can be reduce to second grade fluid filled in a porous space. Thus, the velocity profile for the case of ramped wall temperature is given by

$$\begin{aligned}
 u_{ramp}(y,t) &= H(t) \cos \omega t e^{-\frac{y}{\sqrt{\alpha_3}}} \\
 &+ \frac{H(t)}{2} \sqrt{\frac{L_{26}}{\pi}} \int_0^t \int_0^\infty \frac{y \cos[\omega(t-s)]}{u\sqrt{s}} \\
 &\quad \times e^{-\frac{y^2}{4u} - \frac{1}{\lambda}(s+u\alpha_{21})} I_1(2\sqrt{L_{26}us}) duds \\
 &+ u_{R2}(y,t) - u_{R2}(y,t-1)H(t-1),
 \end{aligned} \tag{63}$$

in which

$$\begin{aligned}
 u_{R2}(y,t) &= \frac{b_{24}}{b_{26}} \int_0^t \ell e^{b_{25}(\ell-t) - \frac{y}{\sqrt{\alpha_3}}} \sinh[b_{26}(t-\ell)] d\ell \\
 &+ \frac{b_{24}}{2b_{26}} \sqrt{\frac{L_{26}}{\pi}} \int_0^t \int_0^\infty \int_0^\infty \frac{y(\ell-s)}{u\sqrt{s}} e^{b_{25}(\ell-t) - \frac{y^2}{4u} - \frac{1}{\lambda}(s+u\alpha_{21})} \\
 &\quad \times \sinh[b_{26}(t-\ell)] I_1(2\sqrt{L_{26}us}) duds d\ell \\
 &- \frac{b_{24}}{b_{26}} \int_0^t e^{b_{25}(\ell-t)} \sinh[b_{26}(t-\ell)] \left(\frac{a_1 y^2}{2} + \ell\right) \operatorname{erfc}\left(\frac{y}{2} \sqrt{\frac{a_1}{\ell}}\right) d\ell \\
 &+ \frac{b_{24}}{b_{26}} \sqrt{\frac{a_1}{\pi}} \int_0^t y \sqrt{\ell} e^{b_{25}(\ell-t) - \frac{a_1 y^2}{4\ell}} \sinh[b_{26}(t-\ell)] d\ell.
 \end{aligned} \tag{64}$$

While, the solution of velocity for isothermal plate in this case can be written as

$$\begin{aligned}
 u_{iso}(y,t) &= H(t) \cos \omega t e^{-\frac{y}{\sqrt{\alpha_3}}} \\
 &+ \frac{H(t)}{2} \sqrt{\frac{L_{26}}{\pi}} \int_0^t \int_0^\infty \frac{y \cos[\omega(t-s)]}{u\sqrt{s}} e^{-\frac{y^2}{4u} - \frac{1}{\lambda}(s+u\alpha_{21})} I_1(2\sqrt{L_{26}us}) duds \\
 &+ \frac{b_{24}}{b_{26}} \int_0^t e^{b_{25}(\ell-t) - \frac{y}{\sqrt{\alpha_3}}} \sinh[b_{26}(t-\ell)] d\ell \\
 &+ \frac{b_{24}}{2b_{26}} \sqrt{\frac{L_{26}}{\pi}} \int_0^t \int_0^\infty \int_0^\infty \frac{y}{u\sqrt{s}} e^{b_{25}(\ell-t) - \frac{y^2}{4u} - \frac{1}{\lambda}(s+u\alpha_{21})} \\
 &\quad \times \sinh[b_{26}(t-\ell)] I_1(2\sqrt{L_{26}us}) duds d\ell \\
 &- \frac{b_{24}}{b_{26}} \int_0^t e^{b_{25}(\ell-t)} \sinh[b_{26}(t-\ell)] \operatorname{erfc}\left(\frac{y}{2} \sqrt{\frac{a_1}{\ell}}\right) d\ell.
 \end{aligned} \tag{65}$$

Here,

$$\begin{aligned}
 \alpha_{21} &= 1 + \frac{\lambda}{K}, \quad \alpha_{24} = Ha + \frac{1}{K}, \quad b_{24} = \frac{Gr}{a_1 \lambda}, \\
 b_{25} &= \frac{a_1 - \alpha_{21}}{2a_1 \lambda}, \quad b_{26} = \frac{\sqrt{(a_1 - \alpha_{21})^2 + 4a_1 \lambda \alpha_{24}}}{2a_1 \lambda}, \quad L_{26} = \frac{1}{\lambda^2} (\alpha_{21} - \lambda \alpha_{24}).
 \end{aligned} \tag{66}$$

However, by making $Ha = 0$, $Rd = 0$, $K \rightarrow \infty$ and $Gr = 1$, the above equations (63) and (65) lead to the following expressions

$$\begin{aligned}
 u_{ramp}(y,t) &= H(t) \cos \omega t e^{-\frac{y}{\sqrt{\lambda}}} \\
 &+ \frac{H(t)}{2} \frac{1}{\lambda \sqrt{\pi}} \int_0^t \int_0^\infty \frac{y \cos[\omega(t-s)]}{u\sqrt{s}} e^{-\frac{y^2}{4u} - \frac{1}{\lambda}(s+u)} I_1\left(\frac{2}{\lambda} \sqrt{us}\right) duds \\
 &+ u_{R3}(y,t) - u_{R3}(y,t-1)H(t-1),
 \end{aligned} \tag{67}$$

where $u_{R3}(y,t)$ is now become

$$\begin{aligned}
 u_{R3}(y,t) = & \frac{2}{Pr-1} \int_0^t e^{b_3(\ell-t) - \frac{y^2}{4\ell}} \sinh\left[\frac{b_3}{\lambda}(t-\ell)\right] d\ell \quad (68) \\
 & + \frac{1}{\lambda\sqrt{\pi}(Pr-1)} \int_0^t \int_0^\infty \int_0^\infty \frac{y(\ell-s)}{u\sqrt{s}} e^{b_3(\ell-t) - \frac{y^2}{4u} - \frac{1}{\lambda}(s+u)} \\
 & \quad \times \sinh\left[\frac{b_3}{\lambda}(t-\ell)\right] I_1\left(\frac{2}{\lambda}\sqrt{us}\right) dudsd\ell \\
 & - \frac{2}{Pr-1} \int_0^t \left(\frac{Pr y^2}{2} + \ell\right) \operatorname{erfc}\left(\frac{y}{2}\sqrt{\frac{Pr}{\ell}}\right) e^{b_3(\ell-t)} \sinh\left[\frac{b_3}{\lambda}(t-\ell)\right] d\ell \\
 & + \frac{2}{Pr-1} \sqrt{\frac{Pr}{\pi}} \int_0^t y\sqrt{\ell} e^{b_3(\ell-t) - \frac{Pr y^2}{4\ell}} \sinh\left[\frac{b_3}{\lambda}(t-\ell)\right] d\ell,
 \end{aligned}$$

and

$$\begin{aligned}
 u_{iso}(y,t) = & H(t) \cos \omega t e^{-\frac{y^2}{4t}} \quad (69) \\
 & + \frac{H(t)}{2} \frac{1}{\lambda\sqrt{\pi}} \int_0^t \frac{y \cos[\omega(t-s)]}{u\sqrt{s}} e^{-\frac{y^2}{4u} - \frac{1}{\lambda}(s+u)} I_1\left(\frac{2}{\lambda}\sqrt{us}\right) dudsd\ell \\
 & + \frac{2}{Pr-1} \int_0^t e^{b_3(\ell-t) - \frac{y^2}{4\ell}} \sinh\left[\frac{b_3}{\lambda}(t-\ell)\right] d\ell \\
 & + \frac{1}{\lambda\sqrt{\pi}(Pr-1)} \int_0^t \int_0^\infty \int_0^\infty \frac{y}{u\sqrt{s}} e^{b_3(\ell-t) - \frac{y^2}{4u} - \frac{1}{\lambda}(s+u)} \\
 & \quad \times \sinh\left[\frac{b_3}{\lambda}(t-\ell)\right] I_1\left(\frac{2}{\lambda}\sqrt{us}\right) dudsd\ell \\
 & - \frac{2}{Pr-1} \int_0^t e^{b_3(\ell-t)} \sinh\left[\frac{b_3}{\lambda}(t-\ell)\right] \operatorname{erfc}\left(\frac{y}{2}\sqrt{\frac{Pr}{\ell}}\right) d\ell.
 \end{aligned}$$

Here, $P \neq$ and the arbitrary constants are given by

$$b_3 = \frac{1}{\lambda Pr}, \quad b_4 = \frac{P - r}{2\lambda Pr} \quad (70)$$

It is noted that, the solution of equation (69) is identical with the published result obtained by Samiulhaq et al. (2014b). This fact is shown in the Fig. 3 where the graph of solution (69) is matched well with the equation (11) in Samiulhaq et al. (2014b). Hence, with this evidence, the accuracy of our finding is confirmed.

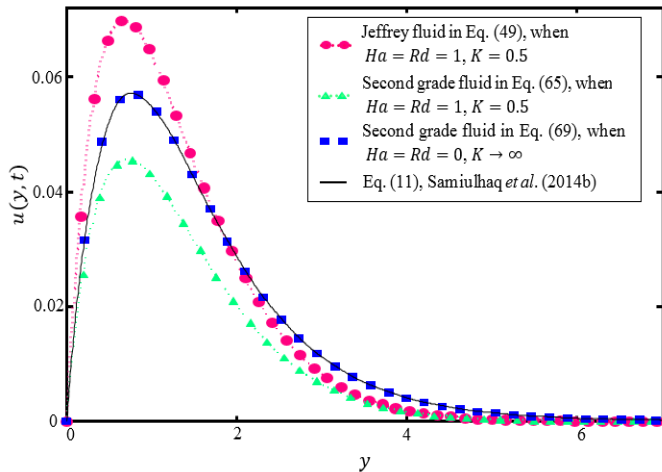


Fig 3. Comparison of velocity profile of an isothermal case in equation (69) with equation (11) obtained by Samiulhaq et al. (2014b) when $\lambda_1 = \lambda = 0$, $Gr = 1$, $P =$ and $t = 0$.

Case 3: Solution for Stokes' First Problem

In addition, by taking $\omega = 0$ into equations (47) and (49) lead to following expression

$$u_r(y,t) = u_{iso}(y,t) + u_3(y,t) \quad (71)$$

$$u_{iso}(y,t) = u_{1a}(y,t) + u_3(y,t) \quad (72)$$

where

$$u_{1a}(y,t) = H(t) e^{-y\sqrt{t}} + \frac{H(t)}{2} \sqrt{\frac{L_6}{\pi}} \int_0^t \int_0^\infty \frac{y}{u\sqrt{s}} e^{-\frac{y^2}{4u} - L_6 s - u L_6} I_1(2\sqrt{L_6 us}) dudsd\ell \quad (73)$$

These solutions correspond to the Stokes' first problem of Jeffrey fluid for case of ramped wall temperature and an isothermal plate over an impulsive motion of the plate, respectively.

RESULTS AND DISCUSSION

The effect of porosity on unsteady MHD free convection flow of Jeffrey fluid corresponding to the cosine oscillation of the plate with ramped wall temperature in the presence of magnetic field and thermal radiation was remarked and the governing equations subjected to initial and boundary conditions (4) was solved analytically by means of Laplace transform technique. In order to reveal the physical interpretation of foregoing parameters such as material parameter of Jeffrey fluid λ_1 , dimensionless Jeffrey fluid parameter λ , phase angle ωt , Hartmann number Ha , Grashof number Gr , permeability parameter K , Prandtl number Pr , radiation parameter Rd and dimensionless time t on the obtained solutions, the numerical results for velocity and temperature are computed and shown graphically in Fig. 4-16. The numerical result for skin friction and Nusselt number are also provided for some physical quantities of interest and analyzed through tabular forms.

Influence of material parameter of Jeffrey fluid λ_1 (when λ are fixed values) on velocity profile is displayed in Fig. 4 for both ramped wall and isothermal cases. From this figure, it is observed that the velocity increase with increasing values of λ_1 for ramped wall temperature and an isothermal plate. However, at certain point, the trend of ramped wall temperature is changed, where the velocity is decreasing as λ_1 increase. On the other hand, in Fig. 5 the effect of dimensionless Jeffrey fluid, λ (when λ_1 are fixed values) on velocity is showed the reverse behavior where an increase of λ slow the motion of the fluid. Similar pattern is noticed in Fig. 6 when both λ_1 and λ are set for a same values.

The variation of phase angle ωt upon velocity is analyzed in Fig. 7. Obviously, the fluid is oscillating between -1 and 1 which shows an oscillatory behaviour. Also, this figure can easily check the accuracy of our results where the obtained solutions (47) and (49) are satisfied the boundary condition given in equation (11). Hence, due to this fact we can say both mathematical and graphical results are found in excellent agreement and we are confident our present results are accurate.

The impact of magnetic field or Hartmann number Ha on velocity profile is demonstrated in Fig. 8. As expected, an increase in Ha reduces the fluid motion. In physical point of view, this is because of the Lorentz force similar to the drag force, which arises due to the application of magnetic field to an electrically conducting fluid and gives rise to a resistance force. Due to this force, the motion of fluid flow in momentum boundary layer tends to retard and thus decrease the fluid velocity.

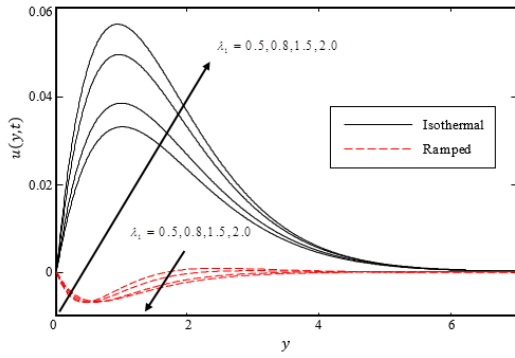


Fig. 4 Velocity profile for different values of λ_1 , when $\lambda = 2$, $\omega t = \pi/2$, $Ha = 2$, $K = 1$, $Gr = 1$, $Pr = 0.71$, $Rd = 2$ and $t = 0.5$.

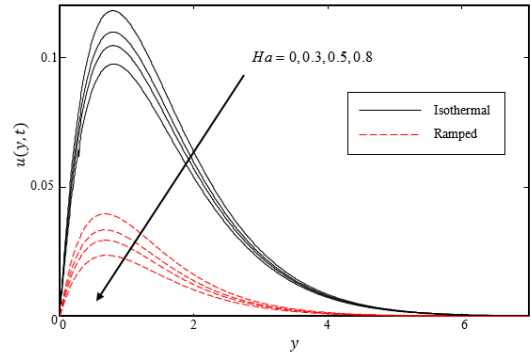


Fig. 8 Velocity profile for different values of Ha , when $\lambda_1 = \lambda = 1$, $\omega t = \pi/2$, $K = 1$, $Gr = 1$, $Pr = 0.71$, $Rd = 2$ and $t = 0.5$.

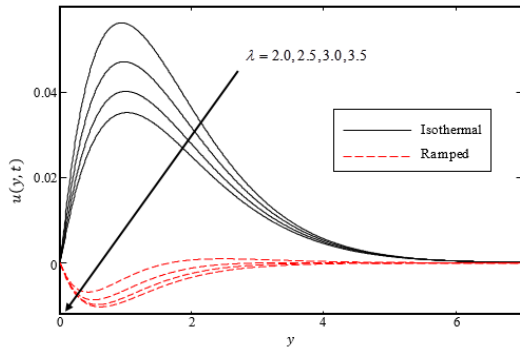


Fig. 5 Velocity profile for different values of λ , when $\lambda_1 = 2$, $\omega t = \pi/2$, $Ha = 2$, $K = 1$, $Gr = 1$, $Pr = 0.71$, $Rd = 2$ and $t = 0.5$.

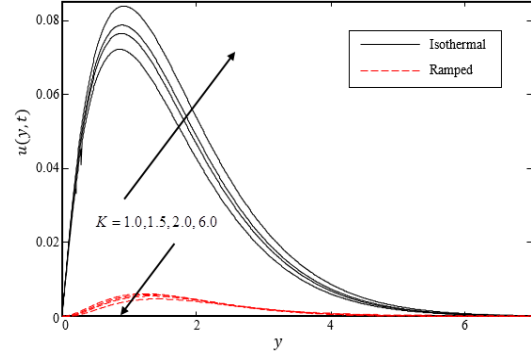


Fig. 9 Velocity profile for different values of K , when $\lambda_1 = \lambda = 1$, $\omega t = \pi/2$, $Ha = 2$, $Gr = 1$, $Pr = 0.71$, $Rd = 2$ and $t = 0.5$.

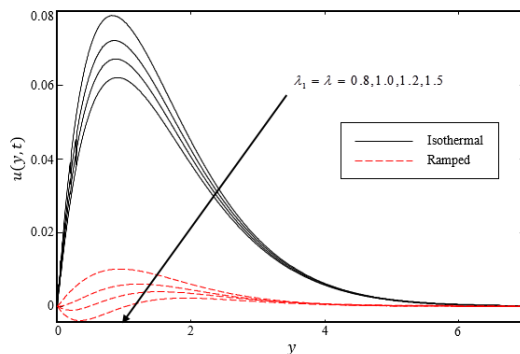


Fig. 6 Velocity profile for different values of Jeffrey fluid parameter, when $\omega t = \pi/2$, $Ha = 2$, $K = 1$, $Gr = 1$, $Pr = 0.71$, $Rd = 2$ and $t = 0.5$.

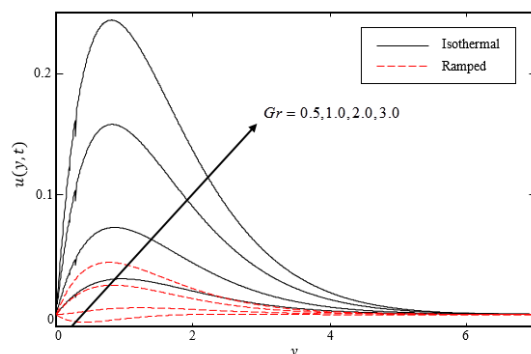


Fig. 10 Velocity profile for different values of Gr , when $\lambda_1 = \lambda = 1$, $\omega t = \pi/2$, $Ha = 2$, $K = 1$, $Pr = 0.71$, $Rd = 2$ and $t = 0.5$.

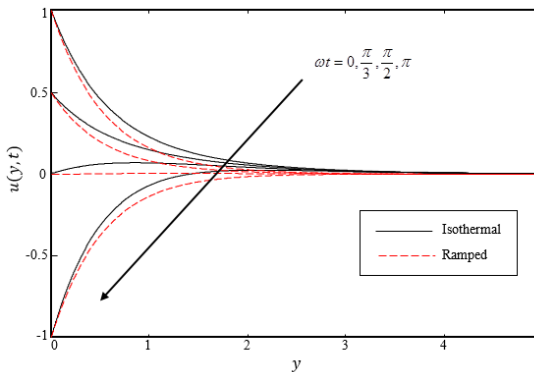


Fig. 7 Velocity profile for different values of ωt , when $\lambda_1 = \lambda = 1$, $Ha = 2$, $K = 1$, $Gr = 1$, $Pr = 0.71$, $Rd = 2$ and $t = 0.5$.

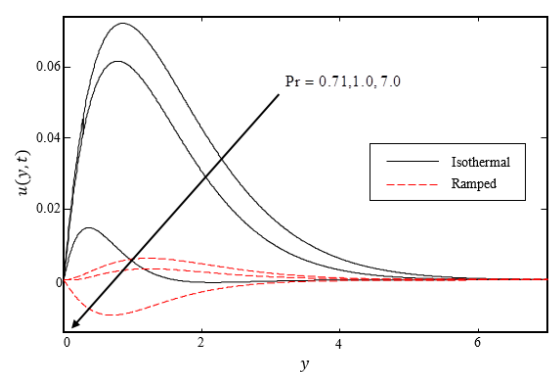


Fig. 11 Velocity profile for different values of Pr , when $\lambda_1 = \lambda = 1$, $\omega t = \pi/2$, $Ha = 2$, $K = 1$, $Gr = 1$, $Rd = 2$ and $t = 0.5$.

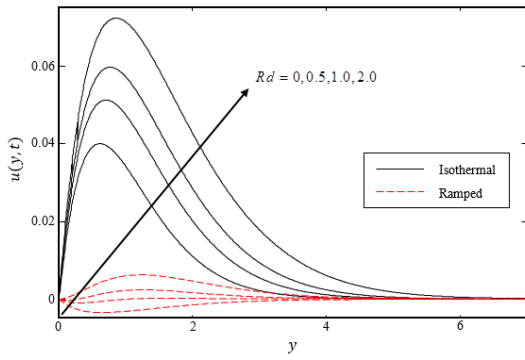


Fig. 12 Velocity profile for different values of Rd , when $\lambda_1 = \lambda = 1$, $\omega t = \pi/2$, $Ha = 2$, $K = 1$, $Gr = 1$, $Pr = 0.71$ and $t = 0.5$.

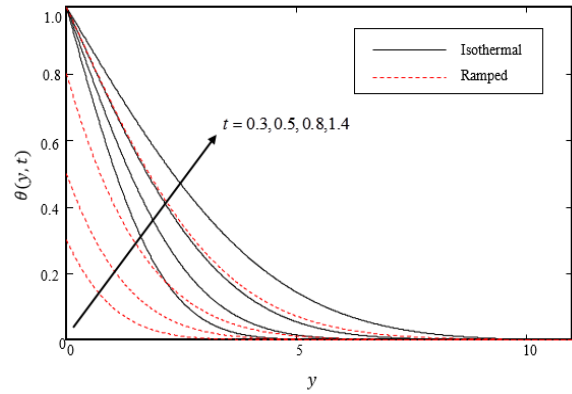


Fig. 16 Temperature profile for different values of t , when $Pr = 0.71$ and $Rd = 2$.

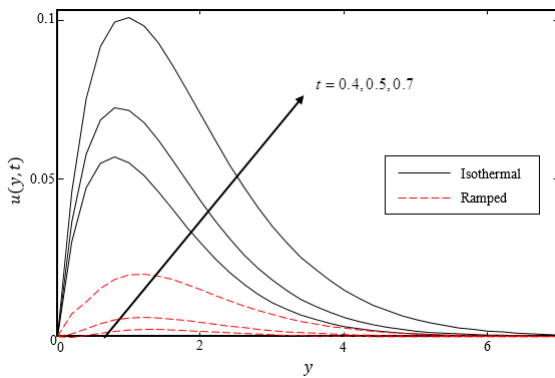


Fig. 13 Velocity profile for different values of t , when $\lambda_1 = \lambda = 1$, $\omega t = \pi/2$, $Ha = 2$, $K = 1$, $Gr = 1$, $Pr = 0.71$ and $Rd = 2$.

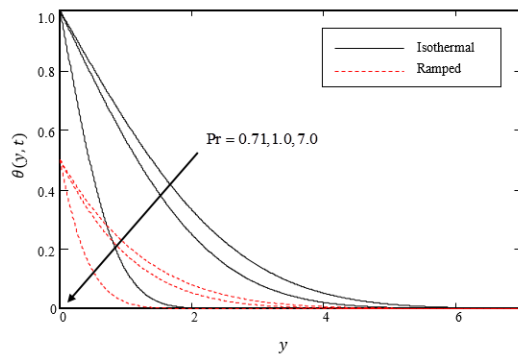


Fig. 14 Temperature profile for different values of Pr , when $Rd = 2$ and $t = 0.5$.

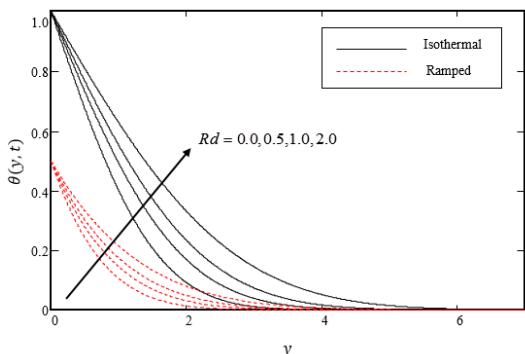


Fig. 15 Temperature profile for different values of Rd , when $Pr = 0.71$ and $t = 0.5$.

Fig. 9 depicts the effect of permeability parameter K on velocity distribution. It is noticed that, as K increase, the velocity for an isothermal case is increase but decrease for the case of ramped wall temperature. Furthermore, from Fig. 10, the influence of Grashof number Gr on velocity field. A rise in Gr to the enhancement of thermal effect which give intensify of the fluid flow.

In addition, the effect of Prandtl number, Pr on velocity is interpreted in Fig. 11. Three different values of $Pr = 0.71, 1.0, 7.0$ are chosen which correspond to air, electrolyte and water respectively. It is found that, the velocity decrease with increasing Pr . This situation occur because of high values of Prandtl number have high viscosity and small conductivity, this will make the fluid thick and consequently decelerate the fluid velocity.

Fig.12 indicates the velocity distribution for various values of radiation parameter Rd . Velocity is clearly enhanced considerably with increasing values of Rd . Physically this is due to the rate of energy transport to the fluid increase as the intensity of radiation parameter increase and thereby the fluid velocity increases. Then, Fig. 13 shows the velocity profile is increasing function of dimensionless time t .

Furthermore, it can be analyzed from Fig. 14 that, the temperature profile is reduced when Pr is increased. Physically, this is because high values of Pr tends to decrease the thermal conductivity which make the heat diffuses more slowly from the plate compared to smaller values of Pr . Thus decrease the temperature distribution.

Meanwhile, Fig. 15 illustrates the influence of radiation Rd on temperature field. As anticipated, an increase in Rd increase the temperature profile since radiation parameter signifies the relative contribution of conduction heat transfer to thermal radiation transfer. Finally, it is found from Fig. 16 that, the temperature profile increase due to an increase in the dimensionless time, t .

The numerical results of Nusselt number and skin friction under varying different emerging parameters are computed from analytical expressions (52), (53), (54), (55) and provided in the form of tables. Table 1 presented the influence of t , Pr and Rd on the Nusselt number which measures the rate of heat transfer at the surface of the plate. It is depicted that, the rate of heat transfer for both ramped wall and isothermal cases decreases for large values of t and Rd , whereas an increase in Pr has shown the opposite effect. Meanwhile, It is clearly seen from Table 2, the skin friction for both cases are enhanced with an increase of Gr and Rd . However, increasing values of Ha , K and Pr reduced the skin friction for ramped wall temperature and an isothermal plate.

Table 1 Variation of Nusselt Number for different values of parameters.

t	Rd	Pr	Nu_{ramp}	Nu_{iso}
0.8	0.5	0.71	0.694	0.434
1.5	0.5	0.71	0.402	0.317
2.0	0.5	0.71	0.322	0.274
1.0	1.0	0.71	0.672	0.336
1.0	1.5	0.71	0.601	0.301
1.0	2.0	0.71	0.549	0.274
1.0	2.0	1.0	0.651	0.326
1.0	2.0	7.0	1.724	0.862
1.0	2.0	100	6.515	3.257

Table 2 Variation of skin friction for several values of parameters when $\lambda_1 = \lambda = 2$, $\omega t = \pi/3$ and $t = 0.5$.

Ha	K	Gr	Rd	Pr	τ_{ramp}	τ_{iso}
1.0	0.5	0.5	0.5	0.71	0.889	1.000
1.5	0.5	0.5	0.5	0.71	0.877	0.985
2.0	0.5	0.5	0.5	0.71	0.865	0.970
2.0	1.0	0.5	0.5	0.71	0.740	0.856
2.0	1.5	0.5	0.5	0.71	0.693	0.814
2.0	2.0	0.5	0.5	0.71	0.668	0.791
2.0	2.0	1.0	0.5	0.71	0.759	1.005
2.0	2.0	1.5	0.5	0.71	0.850	1.219
2.0	2.0	2.0	0.5	0.71	0.941	1.433
2.0	2.0	2.0	1.0	0.71	0.964	1.470
2.0	2.0	2.0	1.5	0.71	0.981	1.495
2.0	2.0	2.0	2.0	0.71	0.995	1.515
2.0	2.0	2.0	2.0	1.0	0.969	1.477
2.0	2.0	2.0	2.0	7.0	0.811	1.185
2.0	2.0	2.0	2.0	100	0.659	0.812

CONCLUSION

The unsteady MHD free convection flow of incompressible Jeffrey fluid past an oscillating vertical plate immersed in a porous medium with ramped wall temperature in the presence of magnetic field and thermal radiation has been studied analytically by Laplace transform technique. Graphical results for velocity and temperature profiles are obtained for embedded parameters and discussed. Corresponding expressions of Nusselt number and skin friction for both ramped wall and isothermal plate are calculated and presented in tables. A comparative study between the present results and the previous work in the sense of limiting cases are provided and a better agreement is gained. The following main points are concluded from this study:

- the boundary layer thickness for ramped wall temperature is always less than isothermal plate.
- An increase in K enhance the fluid flow for an isothermal plate but decelerate the fluid velocity for the case of ramped wall temperature.
- The rising of Ha increase the Lorentz force, which further resist the fluid motion. As a results, it decrease the fluid velocity.
- The presence of Rd leads to an increase the velocity and temperature profiles for both cases.
- Larger values of Pr leads to a reduction in the velocity and temperature.
- Gr acts as a boosting agent for velocity profile for both ramped wall and an isothermal plate due to an increase in buoyancy force.

ACKNOWLEDGEMENT

The authors would like to acknowledge of Higher Education (MOHE) and Research Management Centre-UTM for the financial support through vote number 4F13, 15H80 and 13H74 for this research.

REFERENCES

Aaiza, G., Khan, I., Shafie, S. (2015). Energy transfer in mixed convection mhd flow of nanofluid containing different shapes of nanoparticles in a channel filled with saturated porous medium. *Nanoscale Research Letters*. 10(490): 1-14.

Al- Khafajy, D. G. S. (2016). Effects of heat transfer on MHD oscillatory flow of Jeffrey Fluid with variable viscosity through porous medium. *Advances in Applied Science Research*. 7(3): 179-186.

Ali, A., Asghar, S. (2014). Analytic solution for oscillatory flow in a channel for Jeffrey Fluid. *Journal of Aerospace Engineering*. 27: 644-651.

Ali, F., Khan, I., Shafie, S. (2014). Closed form solutions for unsteady free convection flow of a second grade fluid over an oscillating vertical plate. *PLoS ONE*. 9(2): 1-15.

Bhaskar Reddy, G., Sreenadh, S., Hemadri Reddy, R., Kavitha, A. (2015). Flow of a Jeffrey Fluid between torsionally oscillating disks. *Ain Shams Engineering Journal*. 6: 355-362.

Cortell, R. (2014). Fluid flow and radiative nonlinear heat transfer over a stretching sheet. *Journal of King Saud University-Science*. 26: 161-167.

Das, R. K., Neog, B. C. (2015). MHD flow past a vertical oscillating plate with radiation and chemical reaction in porous medium. *IOSR Journal of Mathematics*. 11(1): 46-50.

Gao, C., Jian, Y. (2015). Analytical solution of magnetohydrodynamic flow of Jeffrey Fluid through a circular microchannel. *Journal of Molecular Liquids*. 211: 803-811.

Ghara, N., Das, S., Maji, S. L., Jana R. N. (2012). Effect of radiation on MHD free convection flow past an impulsively moving vertical plate with ramped wall temperature. *American Journal of Scientific and Industrial Research*. 3(6): 376-386.

Gul, A., Khan, I., Shafie, S., Khalid, A. and Khan, A. (2015). Heat transfer in MHD mixed convection flow of a ferrofluid along a vertical channel. *PLoS ONE*. 10(11): 1-14.

Hayat, T., Mustafa, M. (2010). Influence of thermal radiation on the unsteady mixed convection flow of a jeffrey fluid over a stretching sheet. *Z. Naturforsch.* 65a: 711-719.

Hayat, T., Iqbal, Z., Mustafa, M., Alsaedi, A. (2014). Unsteady flow and heat transfer of jeffrey fluid over a stretching sheet. *Thermal Science*. 18(4): 1069-1078.

Hayat, T., Khan, M., Fakhar, K., Amin, N. (2010). Oscillatory rotating flows of a fractional Jeffrey Fluid filling a porous space. *Journal of Porous Media*. 13(1): 29-38.

Idowu, A. S., Jimoh, A., Ahmed, L. O. (2015a). Effect of heat and mass transfer on MHD oscillatory flow of jeffrey fluid in a porous channel with thermal conductivity and sores. *Journal of Research in National Development*. 13(2):Chapter 30.

Idowu, A. S., Jimoh, A., Ahmed, L. O. (2015b). Impact of heat and mass transfer on MHD oscillatory flow of Jeffrey Fluid in a porous channel with thermal conductivity, dufour and sores. *Journal of Applied Sciences and Environmental Management*. 19(4): 819-830.

Idowu, A. S., Joseph, K. M., Daniel, S. (2013). Effects of heat and mass transfer on unsteady MHD oscillatory flow of Jeffrey Fluid in a horizontal channel with chemical reaction. *IOSR Journal of Mathematics*. 8(5): 74-87.

Joseph, K. M., Magaji, A. S., Peter, A., Tijani, N. Z. (2016). Effect of variable suction on unsteady MHD oscillatory flow of Jeffrey Fluid in a horizontal channel with heat and mass transfer. *Journal of Scientific and Engineering Research*. 3(3): 599-610.

Kavita, K., Ramakrishna Prasad, K., Aruna Kumari B. (2012). Influence of heat transfer on MHD oscillatory flow of Jeffrey Fluid in a channel. *Advances in Applied Science Research*. 3(4): 2312-2325.

Khalid, A., Khan, I., Khan, A., Shafie, S. (2015a). Unsteady MHD free convection flow of casson fluid past over an oscillating vertical plate embedded in a porous medium. *Engineering Science and Technology, an International Journal*. 18: 309-317.

Khan, I. (2015). A note on exact solutions for the unsteady free convection flow of a Jeffrey Fluid. *Zeitschrift für Naturforsch.* 70(6): 272-284.

Khan, I., Ali, F., Sharidan, S., Norzieha, M. (2010). Exact solutions for accelerated flows of a rotating second grade fluid in a porous medium. *World Applied Sciences Journal*. 9: 55-68.

Khan, M., Iftikhar, F., Anjum, A. (2011). Some unsteady flows of a Jeffrey Fluid between two side walls over a plane wall. *Zeitschrift für Naturforsch.* 66a: 745 - 752.

Khan. M. (2007). Partial slip effects on the oscillatory flows of a fractional Jeffrey Fluid in a porous medium. *Journal of Porous Media*. 10(5): 473-487.

Mabood, F., Abdel-Rahman, R., Lorenzini, G. (2016). Numerical study of unsteady Jeffrey fluid flow with magnetic field effect and variable fluid properties. *Journal of Thermal Science and Engineering Applications*. 8: 1-9.

Mekheimer, K. S., Husseny S. Z.-A., Ali A. T., Abo-Elkhair R. E. (2011). Lie Point Symmetries and Similarity Solutions for an Electrically Conducting Jeffrey Fluid. *Physica Scripta*. 83: 1-7.

- Nadeem, S., Tahir, B., Labropulu, F., Akbar, N. S. (2014). Unsteady oscillatory stagnation point flow of a Jeffrey Fluid. *Journal of Aerospace Engineering*. 27: 636-643.
- Narahari, M., Ishak, A. (2011). A radiation effects on free convection flow near a moving vertical plate with newtonian heating. *Journal of Applied Sciences*. 11(7): 1096-1104.
- Pantokratoras, A., Fang, T. (2013). Sakiadis flow with nonlinear Rosseland thermal radiation. *Physica Scripta*. 87: 1-5.
- Qayyum, A., Awais, M., Alsaedi, A., Hayat, T. (2012). Unsteady squeezing flow of Jeffrey Fluid between two parallel disks. *Chinese Physics Letters*. 29(3): 1-4.
- Samiulhaq, Ahmad, S., Vieru, D., Khan, I., Shafie, I. (2014a). Unsteady magnetohydrodynamic free convection flow of a second grade fluid in a porous medium with ramped wall temperature. *PLoS ONE*. 9(5): 1-9.
- Samiulhaq, Khan, I., Ali, F., Shafie, S. (2014b). Free convection flow of a second grade fluid with ramped wall temperature. *Heat Transfer Research*. 45(7): 579-588.
- Sree, H. K., Sudheer Kumar, M., Vijayatha, D. (2016). MHD heat transfer oscillatory flow Jeffrey Fluid in an inclined channel filled with porous medium. *Chemical and Process Engineering Research*. 44: 26-30.
- Sukumar, M., Krishna Murthy, M., Varma, S. V. K., Rajinikanth, K. (2016). Slip effects on MHD flow of Jeffrey Fluid over an unsteady shrinking sheet with wall mass transfer. *Middle-East Journal of Scientific Research*. 24(6): 1920-1925.